Collectivity and manifestations of minimum-bias jets in high-energy nuclear collisions

Thomas A. Trainor[1a]

[1] *CENPA 354290 University of Washington, Seattle, Washington, USA*

Abstract. Collectivity, as interpreted to mean flow of a dense medium in high-energy A-A collisions described by hydrodynamics, has been attributed to smaller collision systems – p-A and even p-p collisions – based on recent analysis of LHC data. However, alternative methods reveal that some data features attributed to flows are actually manifestations of minimum-bias (MB) jets. In this presentation I review the differential structure of single-particle p_t spectra from SPS to LHC energies in the context of a two-component (soft + hard) model (TCM) of hadron production. I relate the spectrum hard component to measured properties of isolated jets. I use the spectrum TCM to predict accurately the systematics of ensemble-mean $\bar{p}_t$ in p-p, p-A and A-A collision systems over a large energy interval. Detailed comparisons of the TCM with spectrum and correlation data suggest that MB jets play a dominant role in hadron production near midrapidity. Claimed flow phenomena are better explained as jet manifestations agreeing quantitatively with measured jet properties.

1 Introduction

Collectivity (interpreted to represent hydrodynamic flows [1]) has been attributed recently to smaller collision systems [2] based on certain correlation phenomena conventionally attributed to flows in larger A-A systems (e.g. v_2 data). But the term "collectivity" simply represents *any* correlated collection: correlations $\Rightarrow$ collectivity. For instance, dijet production represents a collective phenomenon that arguably dominates high-energy nuclear collisions. Several hadron production mechanisms may contribute to observed correlations. It should be our task to identify those mechanisms by comprehensive data analysis based on a variety of methods. The goal is then to extract *all* information from available particle data and interpret that information based on recognized physics principles. In this study measured $\bar{p}_t$ trends for three collision systems are compared to corresponding p_t spectra and measured jet properties.

2 Two-component (soft + hard) model or TCM for A-B collisions

The TCM is a comprehensive and accurate model of hadron production in A-B collisions near midrapidity inferred inductively from p_t spectra [3, 4] and angular correlations [5–7]. For instance, intensive charge density $\bar{\rho}_0$ can be separated into two components: $\bar{\rho}_0 = \bar{\rho}_s + \bar{\rho}_h$ (soft +

---

[a]e-mail: ttrainor99@gmail.com

hard). Based on comprehensive data analysis (e.g. [5, 8, 9]) the two components have been interpreted physically as follows: Soft component SC results from projectile-nucleon dissociation to *participant* low-x gluons $\sim \bar{\rho}_s \equiv n_s/\Delta\eta \propto \log(\sqrt{s}/10 \text{ GeV})$. Hard component HC results from large-angle scattering of participant gluons which then fragment to a minimum-bias (MB) ensemble of dijets. Measured SC and HC (yields, spectra and correlations) are related in p-p collisions via $\bar{\rho}_h \equiv n_h/\Delta\eta \approx \alpha\bar{\rho}_s^2$ (*noneikonal* trend) with $\alpha \approx O(0.01)$. An eikonal trend (e.g. as in the Glauber model of A-A collisions) would instead follow $\bar{\rho}_h \propto \bar{\rho}_s^{4/3}$ [10]. The p-p $\bar{\rho}_h \approx \alpha\bar{\rho}_s^2$ trend is illustrated in Fig. 1 (a) as $n_h/n_s \approx 0.005\,\bar{\rho}_s$ (within $\Delta\eta = 1$) [3].

A TCM for hadron production in A-B collisions follows suite but requires additional geometry parameters defined within the Glauber model of collision geometry based on the eikonal approximation. $N_{part}/2$ is the number of participant nucleon pairs, N_{bin} is the number of N-N binary collisions, and $\nu \equiv 2N_{bin}/N_{part}$ is the mean number of binary collisions per participant pair. For instance, the event-ensemble mean of extensive total P_t (p_t integrated within some acceptance $\Delta\eta$) can be represented in TCM form as $\bar{P}_t = \bar{P}_{ts} + \bar{P}_{th}$ or

$$\bar{P}_t = (N_{part}/2)n_{sNN}\bar{p}_{tsNN} + N_{bin}n_{hNN}\bar{p}_{thNN}; \quad \bar{P}_t/n_s = \bar{p}_{ts} + x(n_s)\nu(n_s)\bar{p}_{thNN}(n_s), \quad (1)$$

where $x \equiv \bar{\rho}_{hNN}/\bar{\rho}_{sNN} = n_{hNN}/n_{sNN}$ and the TCM incorporates factorization of N-N low-x gluon participants (noneikonal) and A-B nucleon participants (eikonal). Note that $\bar{p}_t$ SC $\bar{p}_{tsNN} \to \bar{p}_{ts} \approx 0.4$ GeV/c is observed to be universal for N-N collisions within A-B collisions.

3 Minimum-bias jet manifestations in p-p p_t spectra and correlations

Quantitative correspondence between measured jet properties and single-particle p_t spectra has been demonstrated previously for 200 GeV p-p and Au-Au spectra down to 0.5 GeV/c [8]. The demonstration relies on the observation that jet spectra and fragmentation functions (FFs) have simple universal forms (Gaussian and beta distribution) when plotted on rapidity variables. Some details are reviewed in this section (angular correlations are described below).
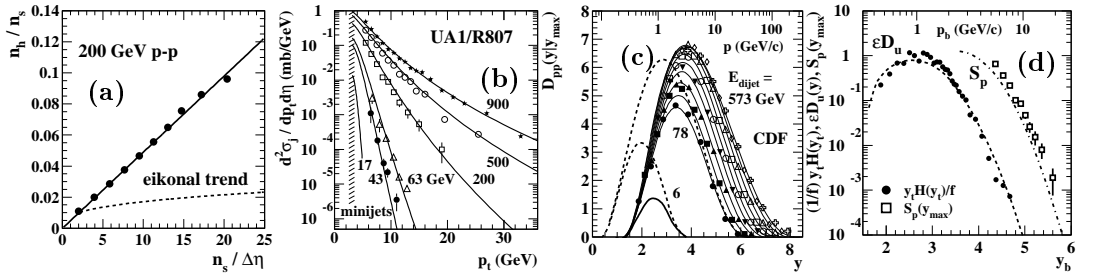

Figure 1. (a) Hard/soft ratio vs soft density $\bar{\rho}_s$. (b) Jet p_t spectra for several energies from the ISR and Sp$\bar{\text{p}}$S. Curves through data are from Ref. [9]. (c) Fragmentation functions from p-$\bar{p}$ collisions described by a simple parametrization from Ref. [9]. (d) Spectrum hard component for 200 GeV NSD p-p collisions (solid points) compared to a fragment distribution as predicted by Eq. (2) (dashed).

Figure 1 (b) shows jet spectra from the ISR (43 and 63 GeV points) and Sp$\bar{\text{p}}$S (remaining data points). The curves are derived from a universal parametrization of jet spectra applicable up to 13 TeV [9]. Panel (c) shows jet FFs from p-$\bar{p}$ collisions obtained by the CDF collaboration plotted on rapidity variable $y = \ln[(E + p)/m_\pi]$. The FFs show self-similar variation with jet

energy making a simple parametrization possible. Schematically, the *fragment distribution* (FD) $P(p)$ describing the contribution to a p_t spectrum from MB dijets (spectrum HC) is the convolution of jet spectrum $P(E)$ for a given *p-p* collision energy and FF ensemble $P(p|E)$

$$P(p) = \int_{E_{min}}^{\infty} dE\, P(p|E)\, P(E), \tag{2}$$

with $E_{min} \approx 3$ GeV established by comparisons with hadron spectra [8, 11]. In panel (d) the dashed curve is $P(d)$. The solid points are the spectrum HC from 200 GeV NSD *p-p* collisions [3]. The open boxes are the 200 GeV UA1 jet spectrum appearing in panel (b). It is notable that the majority of jet fragments appear near 1 GeV/c. If E_{min} is reduced significantly below 3 GeV a large overestimate of the measured FD contribution below 1 GeV/c results, since the jet spectrum scales as $d\sigma_{jet}/dp_t \sim 1/p_t^6$ near that energy.

Two-particle angular correlations have been studied for 200 GeV *p-p* collisions [5–7] and Au-Au collisions [12] within $\Delta\eta = 2$. Measured quantity $\Delta\rho/\sqrt{\rho_{ref}}$ is essentially the number of correlated pairs per final-state hadron; η_Δ and ϕ_Δ are angle difference variables.
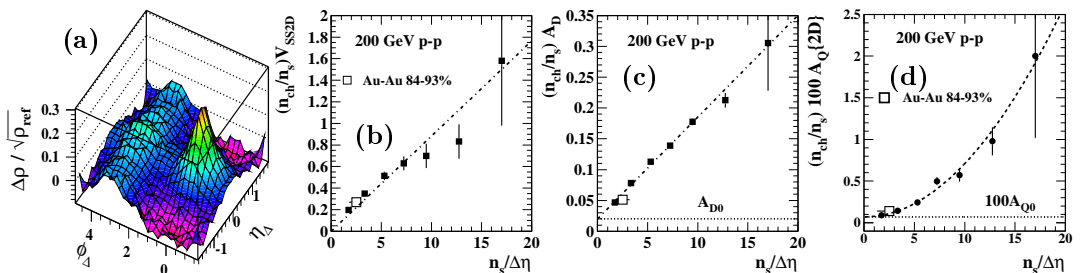

Figure 2. (a) 2D angular correlations for high-multiplicity 200 GeV *p-p* collisions. (b) SS 2D peak volume vs soft density $\bar{\rho}_s$. (c) AS 1D peak amplitude vs density $\bar{\rho}_s$. (d) Quadrupole amplitude A_Q vs $\bar{\rho}_s$. In (b-d) the vertical axis is proportional to number of correlated pairs divided by $\bar{\rho}_s$.

Figure 2 (a) shows angular correlations for high-multiplicity ($\approx 8\bar{\rho}_{0NSD}$) 200 GeV *p-p* collisions with no special p_t cuts. The main features are a SS (same-side on azimuth) 2D peak representing individual jets and an AS (away-side) 1D peak on ϕ_Δ representing back-to-back jet pairs. Superposed on the broader SS peak is a narrower 2D contribution from Bose-Einstein correlations. Just visible is a small SC contribution − a narrow 1D peak on η_Δ.

Figure 2 (b-d) shows systematic variation with n_{ch} or n_s of individual correlation amplitudes obtained by 2D model fits to correlation data [5]. The linear per-hadron trends in panels (b,c) indicate that the correlation hard component (dijets) follows a noneikonal trend: jet-correlated pairs $\propto \bar{\rho}_s^2$ as observed for the *p-p* spectrum HC. Panel (d) shows a quadratic trend on $\bar{\rho}_s$ for *nonjet quadrupole* component A_Q indicating that quadrupole correlated pairs are $\propto \bar{\rho}_s^3$. That trend is actually consistent with the quadrupole trend observed for *A-A* collisions. If $\bar{\rho}_s \sim$ low-x participant gluons and $\bar{\rho}_s^2 \sim$ participant-gluon binary collisions then $\bar{\rho}_s^3 \sim N_{part}N_{bin}$ for *p-p* collisions. The centrality trend observed for the nonjet quadrupole ($\bar{\rho}_0^2 v_2^2$) in Au-Au collisions is $N_{part}N_{bin}\epsilon_{opt}^2$ [13]. Absence of a ϵ_{opt}^2 factor for *p-p* collisions is consistent with the noneikonal $\bar{\rho}_h \propto \bar{\rho}_s^2$ trend: centrality is not relevant for *p-p* collisions.

4 p-p p_t spectrum TCM hard components

The illustrations above pertain to 200 GeV RHIC data as a testbed for MB dijet manifestations in spectra and angular correlations. In preparation for $\bar{p}_t$ analysis the full collision-energy and charge-multiplicity dependence of the spectrum hard component should be understood.

Figure 3 (a) shows the TCM hard components for p-p p_t spectra as a function of collision energy from $\sqrt{s} = 17$ GeV to 13 TeV (curves of various line styles) [4] compared to data for two energies (points) [3, 14]. The TCM spectrum HC model is simple and relies on a few $\log(\sqrt{s})$ terms. The description of spectrum data is in all cases within systematic uncertainties of the data. Spectrum hard components show significant dependence on event multiplicity n_{ch} (e.g. multiple fine lines for the 200 GeV model). For the $\bar{p}_t$ study fiducial hard-component $\bar{p}_{th0}$ values in panel (b) are inferred from a *symmetric* spectrum HC model (for $\bar{\rho}_s \approx 2\bar{\rho}_{sNSD}$) [15].
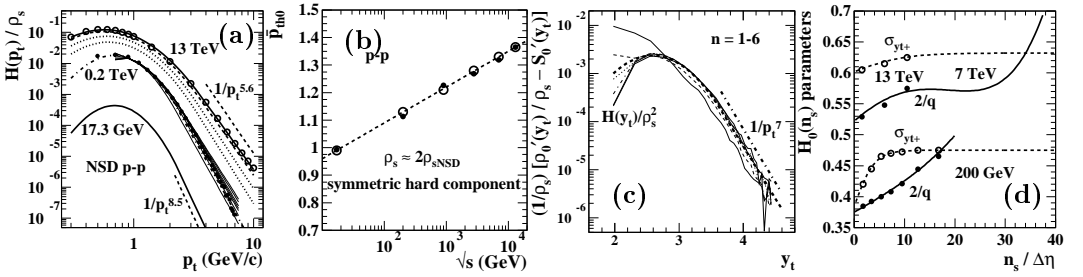

Figure 3. (a) p-p p_t spectrum TCM hard components for several collision energies (curves) compared to data (points). (b) Mean-p_t $\bar{p}_t$ hard components $\bar{p}_{th0}$ inferred from TCM model functions in panel (a). (c) p_t spectrum hard components for several multiplicity classes of 200 GeV p-p collisions. (d) Model parameters $\sigma_{y_{t+}}$ and q for the TCM spectrum hard component, their variation with n_{ch}.

Figure 3 (c) shows spectrum hard components for several n_{ch} classes of 200 GeV p-p collisions [5]. The n_{ch} dependence of the shape has been known for more than ten years [3] and is attributed to bias of the underlying jet energy spectrum in response to the n_{ch} condition. The TCM is modified to accommodate those changes as follows: The hard-component model is a Gaussian plus exponential tail. The transition from Gaussian to exponential is determined by slope matching. The Gaussian widths are treated separately below and above the mode with widths $\sigma_{y_{t-}}$ and $\sigma_{y_{t+}}$ respectively. The exponential constant q is a separate parameter.

Figure 3 (d) shows evolution of spectrum HC model parameters $\sigma_{y_{t+}}$ and q with n_{ch} at 200 GeV and 13 TeV. The trend for the width below the mode $\sigma_{y_{t-}}$ is available in Ref. [4]. For 200 GeV the parameter trends are tightly constrained by spectrum data over the full n_{ch} interval relevant to $\bar{p}_t$ data. For 13 TeV the spectrum data span a more-limited n_{ch} interval. The $2/q$ trend (upper solid curve) has been extended by fitting $\bar{p}_t$ data in the present study.

The $\bar{p}_t$ analysis of Ref. [16] produced uncorrected $\bar{p}'_t$ values, where the prime denotes the effect on spectra of a lower-p_t acceptance cut at $p_{t,min}$ near 0.15 GeV/c. The p_t acceptance cut strongly affects the $\bar{p}_t$ SC but has negligible effect on the HC which is small below 0.5 GeV/c. The relation is $\bar{p}'_{ts} = \bar{p}_{ts}/\xi$ where ξ is the SC efficiency ≈ 0.78 for an *effective* p_t cutoff near 0.17 GeV/c. For universal $\bar{p}_{ts} \approx 0.4$ GeV/c uncorrected $\bar{p}'_{ts} \approx 0.51 \pm 0.2$ GeV/c.

5 p-p $\bar{p}_t$ TCM analysis

The TCM for $\bar{p}_t$ data from p-p collisions is constructed as follows [15]: The uncorrected yield n'_{ch} within angular acceptance $\Delta\eta$ relative to the corrected soft component n_s is $n'_{ch}/n_s = \xi + x(n_s)$ with $\xi = 0.76$ - 0.80 (depending on the effective $p_{t,min}$). For noneikonal p-p collisions $x(n_s, \sqrt{s}) \equiv n_h/n_s \approx \alpha(\sqrt{s})\bar{\rho}_s$ and $\alpha(\sqrt{s})$ is predicted from jet characteristics [4]. The TCM for uncorrected $\bar{p}'_t$ is the first of

$$\bar{p}'_t \equiv \frac{\bar{P}'_t}{n'_{ch}} \approx \frac{\bar{p}_{ts} + x(n_s, \sqrt{s})\,\bar{p}_{th}(n_s, \sqrt{s})}{\xi + x(n_s, \sqrt{s})}; \quad \frac{n'_{ch}}{n_s}\bar{p}'_t \approx \frac{\bar{P}_t}{n_s} = \bar{p}_{ts} + x(n_s, \sqrt{s})\,\bar{p}_{th}(n_s, \sqrt{s}), \tag{3}$$

where $\bar{p}_{ts} \approx 0.4$ GeV/c and $p_{th}(n_s, \sqrt{s})$ is the new information derived from p-p $\bar{p}_t$ data.
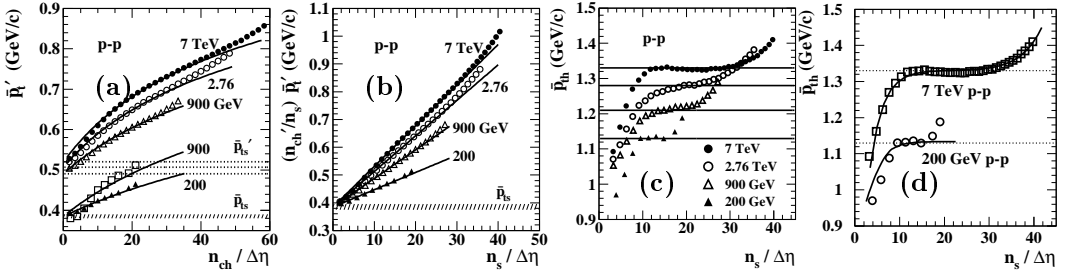

Figure 4. (a) Uncorrected $\bar{p}'_t$ data (points) from Ref. [16] vs the $\bar{p}_t$ TCM (solid curves). (b) Corrected $\bar{P}_t/n_s$ data (points) vs the TCM (solid lines). (c) $\bar{p}_{th}(n_s, \sqrt{s})$, trends vs $\bar{\rho}_s$ for four energies. (d) $\bar{p}_{th}(n_s, \sqrt{s})$, trends for 200 GeV and 7 TeV (points) compared to TCM trends from spectra (curves).

Figure 4 (a) shows uncorrected $\bar{p}'_t$ data from Ref. [16] (upper points) compared to nominally corrected data from STAR and UA1 (lower points). The $\bar{p}'_{ts}$ values for uncorrected data are in the range 0.49 - 0.525 GeV/c as expected (dotted lines). The solid curves are TCM trends assuming no n_{ch} variation of $\bar{p}_t$ hard component [held fixed at values $\bar{p}_{th0}$ from Fig. 3 (b)]. Figure 4 (b) shows corrected $\bar{P}_t/n_s$ data (points) according to the second of Eqs. (3). In that format the TCM is a straight line with slope $\alpha(\sqrt{s})\,\bar{p}_{th0}$ predicted from p_t spectra and jet data.

Figure 4 (c) shows $\bar{p}_{th}(n_s, \sqrt{s})$ data inferred from the uncorrected $\bar{p}'_t$ data according to Eqs. (3). The horizontal lines are the $\bar{p}_{th0}(\sqrt{s})$ values appearing in Fig. 3 (b). Clearly evident are substantial variations with n_s or $\bar{\rho}_s$. However, such variations are expected based on previous spectrum studies as in Refs. [3, 4]. Figure 4 (d) shows $\bar{p}_{th}(n_s)$ values for 200 GeV and 7 TeV (points) compared to a TCM including HC n_{ch} dependence according to Fig. 3 (d). The correspondence between TCM and $\bar{p}_t$ data is within data uncertainties. Accurate correspondence between p-p $\bar{p}_t$ data and the TCM compels the conclusion that there is a direct, quantitative correspondence among measured isolated-jet properties, p_t spectrum hard components and $\bar{p}_t$ data. p-p collisions are dominated by MB dijets and are noneikonal.

6 p-Pb $\bar{p}_t$ TCM analysis

For a TCM description of p-Pb collisions [15] the composite structure of the Pb nucleus must be incorporated by adding *mean participant pathlength* $\nu(n_s) \equiv 2N_{bin}/N_{part}$ as a geometry measure, so for instance $n'_{ch}/n_s \to \xi + x(n_s)\nu(n_s)$. The soft-component charge density

factorizes as $\bar{\rho}_s \equiv (N_{part}/2)\bar{\rho}_{sNN}(n_s)$, similarly $\bar{\rho}_h \equiv N_{bin}\bar{\rho}_{hNN}(n_s)$ and hard/soft ratio $x(n_s) \rightarrow \bar{\rho}_{hNN}(n_s)/\bar{\rho}_{sNN}(n_s) \approx \alpha\bar{\rho}_{sNN}(n_s)$ averaged over N-N collisions as for p-p collisions. Combining those relations gives $N_{part}(n_s)/2 = \alpha\bar{\rho}_s/x(n_s)$, and for p-A collisions $N_{part} \equiv N_{bin} + 1$. Thus, if a model for $x(n_s)$ is specified then N_{part}, N_{bin} and ν are also defined. As described below, $x(n_s)$ for more-peripheral p-A collisions is based on the noneikonal p-p trend and is then extrapolated to more-central collisions with $N_{part}/2 > 1$ based on $\bar{p}_t$ data. The TCM for p-Pb $\bar{p}'_t$ data is similar to Eqs. (3) but with additional $\nu(n_s)$ factors

$$\bar{p}'_t \equiv \frac{\bar{P}'_t}{n'_{ch}} \approx \frac{\bar{p}_{ts} + x(n_s)\nu(n_s)\,\bar{p}_{thNN}(n_s)}{\xi + x(n_s)\nu(n_s)}; \quad \frac{\bar{P}_t(n_s)}{n_s} = \bar{p}_{ts} + x(n_s)\nu(n_s)\,\bar{p}_{thNN}(n_s) \quad (4)$$

assuming $\bar{p}_{thNN}(n_s) \approx \bar{p}_{th0}$ (p-p values) for p-Pb collisions (no jet modification in p-A).
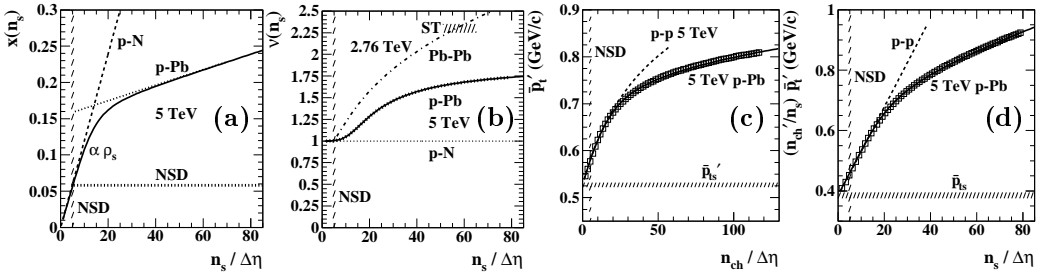

Figure 5. (a) TCM parameter $x(n_s)$ vs $\bar{\rho}_s$ for 5 TeV p-Pb collisions. (b) Corresponding $\nu(n_s)$ trend. (c) Uncorrected $\bar{p}'_t$ data (points) from Ref. [16] vs the $\bar{p}_t$ TCM (solid curve). (d) Corrected $\bar{P}_t/n_s$ data (points) vs the TCM (solid curve). Equivalent p-p trends are included for comparison.

Figure 5 (a) shows a $x(n_s)$ model for p-Pb collisions (solid curve): the observed p-p trend (dashed line) is smoothly transitioned to a second linear trend with reduced slope (dotted line). The additional p-Pb model parameters are $(\bar{\rho}_{s0}, m_0)$, a transition point and slope-reduction factor. Panel (b) shows the corresponding $\nu(n_s)$ trend (solid curve) defined by $x(n_s)$ as noted above. The dash-dotted curve is a Pb-Pb $\nu(n_s)$ trend for comparison.

Figure 5 (c) shows uncorrected $\bar{p}'_t$ data from Ref. [16] (points) with $\bar{p}'_{ts} \approx 0.525$ GeV/c. The solid curve is the TCM defined by Eq. (4) (first) with $\bar{\rho}_{s0} = 15$ and $m_0 = 0.1$ adjusted to accommodate $\bar{p}'_t$ data and $\bar{p}_{thNN}(n_s) \rightarrow \bar{p}_{th0} = 1.30$ GeV/c from Fig. 3 (b). The dashed curve is the p-p TCM for 5 TeV. Figure 5 (d) shows the same features for corrected $\bar{P}_t/n_s$ data with TCM described by Eq. (4) (second). This p-Pb exercise illustrates the transition from noneikonal p-p or p-N trend to eikonal p-A trend with increasing multiplicity. The value of $N_{part}/2$ remains near one (p-N only) up to the transition point but then slowly increases as greater p-A centrality becomes competitive to deliver larger overall charge multiplicity.

7 Pb-Pb $\bar{p}_t$ TCM analysis

For the Pb-Pb $\bar{p}_t$ TCM published yield measurements and a Glauber model based on the eikonal approximation can be used to determined some TCM model elements. Parameter $x(n_s)$ can be derived from *per-participant-pair* charge-density data based on the TCM

$$(2/N_{part})dn_{ch}/d\eta \approx (2/N_{part})\bar{\rho}_0(\nu) \quad = \quad \bar{\rho}_{sNN}[1 + x(\nu)\nu]. \quad (5)$$

Parameter $\nu(n_s)$ can be derived from the Glauber model in the form $\nu(n_s) \approx (N_{part}/2)^{1/3}$ [10] with $N_{part}/2 \approx \bar{\rho}_s/\bar{\rho}_{sNN}$ as in the previous section and $\bar{\rho}_{sNN} \approx \bar{\rho}_{sNSD}$ in both cases.

Figure 6 (a) shows per-participant-pair yield data from Ref. [17] (points). The dashed line is a Glauber linear superposition (GLS) model representing no jet modification. The upper bold dotted curve shows the expected effect of multiplicity fluctuations for more-central A-A collisions [18]. The solid curve is the TCM in Eq. (5) with $x(\nu)$ defined below. Panel (b) shows solution of Eq. (5) for parameter $x(\nu)$ (points) assuming $\bar{\rho}_{sNN} \to \bar{\rho}_{sNSD} \approx 4.6$ [4]. A *sharp transition* (ST), first observed for Au-Au jet-related 2D angular correlations [12], representing evidence of jet modification in the yield trend [8] is evident. The bold dotted curve is a simple TCM expression for $x(\nu)$ that starts from the NSD p-p value $x_{pp} \approx 0.045$, increases rapidly through the ST and maintains a saturation value ≈ 0.142 for more-central collisions, approximately threefold increase over the NSD value. The dashed curve is the equivalent for 200 GeV Au-Au collisions. The interval $\bar{\rho}_s = 10$ - 40 is not well-defined *a priori* by yield data so a TCM expression is required that includes an adjustable x_{pp} [15]

$$x(\nu) = x_{pp} + (0.142 - x_{pp}) \left\{1 + \tanh[(\nu - 2.3)/0.5]\right\}/2, \qquad (6)$$
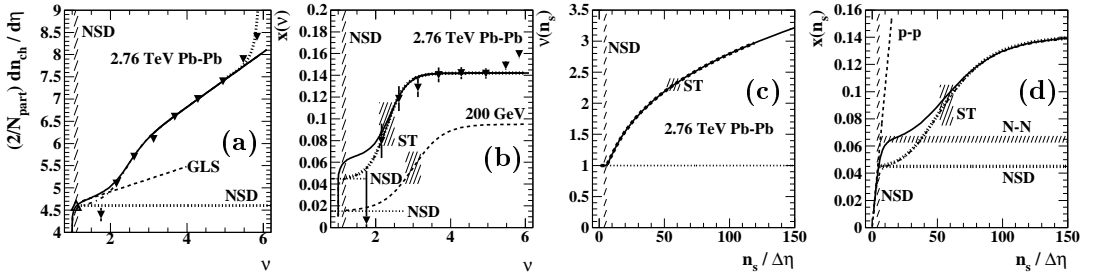
with ST near $\nu = 2.3$.

Figure 6. (a) Per-participant-pair charge density vs centrality measure ν (points) from Ref. [17] compared to the TCM (solid curve). (b) Data from panel (a) transformed to TCM parameter $x(\nu)$ compared to the TCM of Eq. (6) (solid, bold-dotted curves). (c) Glauber parameter $\nu(n_s)$ defined in the text. (d) Parameter $x(\nu)$ from panel (b) transformed to $x(n_s)$ based on $\nu(n_s)$ in panel (c).

Figure 6 (c) shows $\nu(n_s) \approx (\bar{\rho}_s/\bar{\rho}_{sNSD})^{1/3}$ with lower bound $\nu = 1$. Panel (d) shows $x(n_s) = x[\nu(n_s)]$ based on Eq. (6) and panel (c). For this model peripheral Pb-Pb follows the p-p trend (dashed line) for the most peripheral collisions, and more-central Pb-Pb shows the ST feature (jet modification). Yield data do not indicate where the transition from noneikonal p-p to eikonal Glauber trend occurs, requiring the adjustable x_{pp} parameter in Eq. (6).

Figure 7 (a) shows uncorrected $\bar{p}'_t$ data for 2.76 TeV Pb-Pb collisions from Ref. [16] (open squares). The uncorrected soft component is $\bar{p}'_{ts} \approx 0.51$ GeV/c. Data for p-p collisions are also shown (open circles). The Pb-Pb $\bar{p}_t$ TCM (solid curve) follows the p-Pb TCM in Eq. (4) (first) but with the $\nu(n_s)$ and $x(n_s)$ models in Fig. 6 (c,d). The dashed curve is the corresponding TCM for p-p data. The dash-dotted curve is a GLS model assuming no jet modification.

Figure 7 (b) shows product $x(n_s)\bar{p}_{thNN}(n_s) \approx \bar{P}_{thNN}/n_{sNN}$ (open squares) obtained from the data in panel (a) according to Eqs. (4) given the $\nu(n_s)$ model in Fig. 6 (c). The open circles are corresponding p-p data. The solid curve is the Pb-Pb TCM and the dashed curve is the p-p TCM. Note that the ST is clearly evident in this more-differential plot format, but

not in panel (a). The Pb-Pb data follow the p-p trend closely up to and even beyond the NSD $\bar{\rho}_s$ value (vertical hatched band).
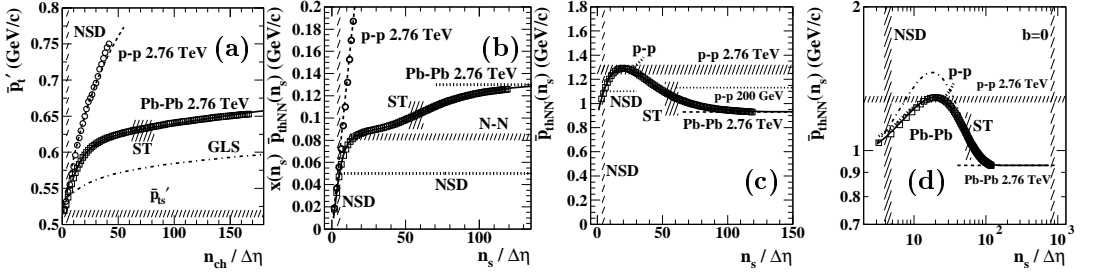

Figure 7. (a) Uncorrected $\bar{p}'_t$ data (points) from Ref. [16] vs the $\bar{p}_t$ TCM (solid curve). p-p data (open circles) and TCM (dashed curve) are included for comparison. The GLS curve represents the Pb-Pb trend for no jet modification. (b) Product $x(n_s)\,\bar{p}_{thNN}(n_s)$ obtained from the data in panel (a) by solving Eq. (4) using $\nu(n_s)$ in Fig. 6 (c). (c) $\bar{p}_{thNN}(n_s)$ obtained from data in panel (b) using $x(n_s)$ in Fig. 6 (d). (d) Panel (c) plotted in log-log format emphasizing the most-peripheral interval.

Figure 7 (c) shows $\bar{p}_{thNN}(n_s)$ data (points) obtained from panel (b) using the $x(n_s)$ model from Fig. 6 (d). The inferred $\bar{p}_{thNN}(n_s)$ values follow the p-p trend (bold dotted curve just visible) for peripheral Pb-Pb but then descend through the ST to a saturation value that is about 75 % of the maximum. The constant saturation values for $x(n_s)$ and $\bar{p}_{thNN}(n_s)$ extend from just above the ST ($\bar{\rho}_s \approx 100$) to central collisions ($\bar{\rho}_s \approx 850$) suggesting that jets do not undergo further alteration within that interval. Panel (d) shows the same features in a log-log format providing better access to peripheral details and extending the plot to central Pb-Pb collisions. The correspondence between p-p (dotted curve) and Pb-Pb data (open squares) up to $\bar{\rho}_s \approx 20$ ($4 \times \bar{\rho}_{sNSD}$) is evident. The dash-dotted curve marks where the data would lie if the bold dotted curve in Fig. 6 (d) were used for $x(n_s)$. The data were actually transformed using the solid curve in that panel with $x_{pp} \to 0.065$ in Eq. (6), 1.45 times the NSD value. The solid curve through the $\bar{p}_{thNN}(n_s)$ data, representing new information obtained from Pb-Pb $\bar{p}_t$ data, is a parametrization that forms the third element of the Pb-Pb $\bar{p}_t$ TCM [15].

8 Comment on Glauber-model analysis of p-Pb collision centrality

The TCM for p-Pb $\bar{p}_t$ data described in Sec. 6 and Ref. [15] can be compared with a recent Glauber analysis of 5 TeV p-Pb centrality in Ref. [19]. For the Glauber analysis it is assumed that integrated charge multiplicity is proportional to Glauber N_{part}: "[n_{ch}] at mid-rapidity scales linearly with [N_{part}]." That assumption is equivalent to assuming that a probability (i.e. event-frequency) distribution on charge multiplicity $- dP/dn_{ch} -$ is equivalent to a fractional cross-section distribution on $N_{part} - (1/\sigma_0)d\sigma/dN_{part} -$ inferred from a Glauber Monte Carlo.

Figure 8 (a) shows an event-frequency distribution (histogram) on VOA amplitude (charge multiplicity within a pseudorapidity interval in the Pb hemisphere) from Ref. [19]. The assumption $N_{part} \propto n_{ch}$ is equivalent to $dP/dn_{ch} \sim (1/\sigma_0)d\sigma/dN_{part}$ as noted above, and the fractional cross sections in the form $100(1 - \sigma/\sigma_0)$ noted in the panel and apparently obtained from a running integral of the histogram seem to be consistent with that statement.

Figure 8 (b) shows Glauber estimates of $(2/N_{part})dn_{ch}/d\eta$ from Ref. [19] (solid points) compared to the TCM equivalent for p-p (dashed) and p-Pb (solid) collisions from Ref. [15] as

reported above. The large discrepancy is apparent. Given N_{part} and N_{bin} from the Glauber analysis corresponding values of ν are plotted in panel (c) (solid dots). The TMC equivalent is the solid curve, and the Glauber trend for Pb-Pb collisions is shown as the dashed curve. That ν for p-Pb collisions might anywhere greatly exceed that for Pb-Pb collisions is notable.
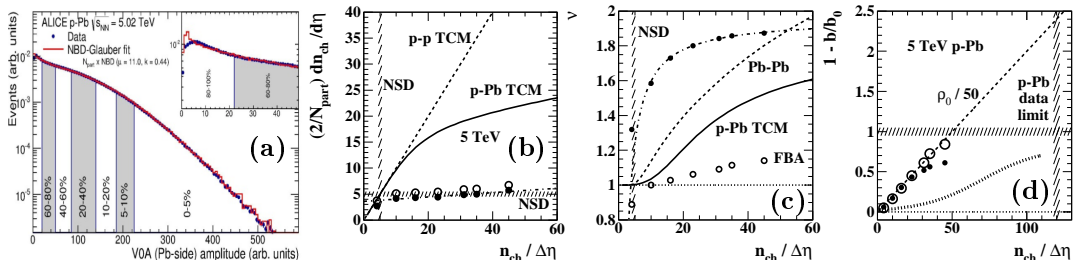

Figure 8. (a) Event-frequency distribution on charge multiplicity in a VOA detector with centrality intervals assigned by p-Pb Glauber analysis [19]. (b) Per-participant-pair p-Pb yields inferred from the Glauber analysis (solid points) and from the present study (solid curve). (c) Participant path length ν inferred from the Glauber analysis (solid points) and the present study (solid curve). Pb-Pb Glauber results (dashed) are included for comparison. (d) Fractional impact parameter in the form $1 - b/b_0$ inferred from the Glauber study (solid points) and indirectly from fractional cross sections in panel (a) (open circles) compared to a trend suggested by the present study (bold dotted curve).

Figure 8 (d) shows fractional impact parameter in the form $1 - b/b_0$ (open circles) inferred from the fractional cross sections in panel (a) assuming that $\sigma/\sigma_0 = (b/b_0)^2$. The solid dots are the same quantity based on b values from the Glauber analysis and assuming that $b_0 \approx 7.1 + 0.85 \approx 8$ fm. Whereas the Glauber analysis in Ref. [19] reports 0-5% central p-Pb collisions for $\bar{\rho}_0 \approx 45$ the p-Pb $\bar{p}_t$ data from Ref. [16] (same collaboration) extend to $\bar{\rho}_0 \approx 120$, nearly three times larger. The bold dotted curve suggests a more realistic trend for b/b_0.

The basic problem with the analysis in Ref. [19] is the initial assumption $N_{part} \propto n_{ch}$ which is strongly violated for p-Pb collisions. Just as for p-p collisions in Sec. 5 initial increase of the n_{ch} condition is more easily met in p-Pb collisions by higher multiplicities in individual p-N collisions than by increasing p-Pb centrality. $N_{part}/2 \approx 1$ persists until $\bar{\rho}_{s0} \approx 15$, three times the NSD value. Only then does $N_{part}/2$ begin to increase above 1 significantly. Below that point $d\sigma/dn_{ch} \approx 0$ and p-Pb "centrality" remains fixed at 100%. The correct relation is

$$d\sigma/dn_{ch} = (dN_{part}/dn_{ch})d\sigma/dN_{part}, \tag{7}$$

where $d\sigma/dN_{part}$ may be obtained from a Glauber Monte Carlo but the Jacobian dN_{part}/dn_{ch} is determined by the p-Pb $\bar{p}_t$ TCM as described above. As noted, the Jacobian factor is essentially zero over a substantial n_{ch} interval below transition point $\bar{\rho}_{s0}$ in Sec. 6. Based on the assumption in Ref. [19] the Jacobian would have a fixed value near $2/n_{chNSD}$ for all n_{ch}.

9 Summary

Recently, claims have emerged that hydrodynamic flows must play a role in smaller collision systems (p-A and even p-p) based on observation of the same phenomena in those systems attributed to flows in more-central A-A systems. However, the argument could be reversed to conclude that if phenomena appear in collision systems so small and low-density that

flows arising from particle rescattering are impossible then the same phenomena observed in more-central A-A may not represent flows. Recent $\bar{p}_t$ data may contribute to a resolution.

The two-component (soft + hard) model (TCM) of hadron production near midrapidity provides an accurate and comprehensive description of yield, spectrum and correlation data applicable to any A-B collision system. While one or more other mechanisms may contribute to hadron production in minor ways (e.g. a nonjet quadrupole component) projectile-nucleon dissociation (soft) and dijet production (hard) appear as the dominant processes in all cases.

From TCM analysis of $\bar{p}_t$ data described above for three successive collision systems the following may be concluded: (a) p-p $\bar{p}_t(n_s, \sqrt{s})$ hard-component trends agree with spectrum HC evolution and measured MB dijet properties. (b) p-p dijet production is *noneikonal*, p-p centrality is not relevant. (c) The p-Pb $\bar{p}_{th}(n_s)$ hard component establishes factorization of A-B Glauber and N-N noneikonal trends. (d) p-Pb $\bar{p}_t$ data confirm that MB dijets dominate $\bar{p}_t(n_s)$ variation. (e) In effect, MB dijets probe the centrality evolution of p-Pb collisions with n_{ch}. (f) Pb-Pb $\bar{p}_t$ data confirm that the Glauber model effectively describes more-central A-A collisions, but peripheral collisions accurately follow p-p (i.e. N-N) trends. (g) The Pb-Pb $\bar{p}_{thNN}(n_s)$ trend confirms that jets are *modified* quantitatively above the ST, but jets still dominate spectrum and correlation structure in more-central Pb-Pb collisions.

Thus, the likelihood that flows play any role in small collision systems appears negligible. Claimed novel phenomena may be better explained either as due to MB dijets or as a related QCD process (e.g. multipole radiation). The same argument may be extended even to the most-central A-A collisions at the highest energies. Before novelty is claimed the contribution of MB dijets and related QCD processes to data trends must first be well understood.

References

[1] P. Huovinen and P. V. Ruuskanen, Ann. Rev. Nucl. Part. Sci. **56**, 163 (2006).

[2] K. Dusling, W. Li and B. Schenke, Int. J. Mod. Phys. E **25**, no. 01, 1630002 (2016).

[3] J. Adams *et al.* (STAR Collaboration), Phys. Rev. D **74**, 032006 (2006).

[4] T. A. Trainor, J. Phys. G **44**, 075008 (2017).

[5] T. A. Trainor and D. J. Prindle, Phys. Rev. D **93**, 014031 (2016).

[6] R. J. Porter and T. A. Trainor (STAR Collaboration), J. Phys. Conf. Ser. **27**, 98 (2005).

[7] R. J. Porter and T. A. Trainor (STAR Collaboration), PoS **CFRNC2006**, 004 (2006).

[8] T. A. Trainor, Phys. Rev. C **80**, 044901 (2009).

[9] T. A. Trainor, Phys. Rev. D **89**, 094011 (2014).

[10] T. A. Trainor and D. J. Prindle, hep-ph/0411217.

[11] T. A. Trainor, J. Phys. G **42**, no. 8, 085105 (2015).

[12] G. Agakishiev, *et al.* (STAR Collaboration), Phys. Rev. C **86**, 064902 (2012).

[13] D. T. Kettler (STAR collaboration), Eur. Phys. J. C **62**, 175 (2009).

[14] J. Adam *et al.* (ALICE Collaboration), Phys. Lett. B **753**, 319 (2016).

[15] T. A. Trainor, arXiv:1708.09412.

[16] B. B. Abelev *et al.* (ALICE Collaboration), Phys. Lett. B **727**, 371 (2013).

[17] K. Aamodt *et al.* (ALICE Collaboration), Phys. Rev. Lett. **106**, 032301 (2011).

[18] T. A. Trainor, Phys. Rev. C **91**, 044905 (2015)

[19] J. Adam *et al.* (ALICE Collaboration), Phys. Rev. C **91**, no. 6, 064905 (2015).